



This is a repository copy of *The acoustical properties of tetraethyl orthosilicate based granular silica aerogels*.

White Rose Research Online URL for this paper:
<https://eprints.whiterose.ac.uk/175557/>

Version: Published Version

Article:

Begum, H., Horoshenkov, K.V. orcid.org/0000-0002-6188-0369, Conte, M. orcid.org/0000-0002-1399-0344 et al. (5 more authors) (2021) The acoustical properties of tetraethyl orthosilicate based granular silica aerogels. *The Journal of the Acoustical Society of America*, 149 (6). pp. 4149-4158. ISSN 0001-4966

<https://doi.org/10.1121/10.0005200>

Reuse

This article is distributed under the terms of the Creative Commons Attribution (CC BY) licence. This licence allows you to distribute, remix, tweak, and build upon the work, even commercially, as long as you credit the authors for the original work. More information and the full terms of the licence here:
<https://creativecommons.org/licenses/>

Takedown

If you consider content in White Rose Research Online to be in breach of UK law, please notify us by emailing eprints@whiterose.ac.uk including the URL of the record and the reason for the withdrawal request.



eprints@whiterose.ac.uk
<https://eprints.whiterose.ac.uk/>

The acoustical properties of tetraethyl orthosilicate based granular silica aerogels

H. Begum, K. V. Horoshenkov, M. Conte, W. J. Malfait, S. Zhao, M. M. Koebel, P. Bonfiglio, and R. Venegas

Citation: *The Journal of the Acoustical Society of America* **149**, 4149 (2021); doi: 10.1121/10.0005200

View online: <https://doi.org/10.1121/10.0005200>

View Table of Contents: <https://asa.scitation.org/toc/jas/149/6>

Published by the [Acoustical Society of America](#)

ARTICLES YOU MAY BE INTERESTED IN

[A series approximation to the Kirchhoff integral for Gaussian and exponential roughness covariance functions](#)
The Journal of the Acoustical Society of America **149**, 4239 (2021); <https://doi.org/10.1121/10.0005282>

[The mechanical potential of ultrasound on nervous tissue](#)
The Journal of the Acoustical Society of America **149**, R11 (2021); <https://doi.org/10.1121/10.0005066>

[Experimental investigation of low Reynolds number rotor noise](#)
The Journal of the Acoustical Society of America **149**, 3813 (2021); <https://doi.org/10.1121/10.0005068>

[Acoustic streaming induced by MHz-frequency ultrasound extends the volume limit of cell suspension culture](#)
The Journal of the Acoustical Society of America **149**, 4180 (2021); <https://doi.org/10.1121/10.0005197>

[Acoustic measurement and statistical characterization of direct-printed, variable-porosity aluminum foams](#)
The Journal of the Acoustical Society of America **149**, 4327 (2021); <https://doi.org/10.1121/10.0005273>

[Acoustics modelling of open-cell foam materials from microstructure and constitutive properties](#)
The Journal of the Acoustical Society of America **149**, 2016 (2021); <https://doi.org/10.1121/10.0003824>

CALL FOR PAPERS

JASA
THE JOURNAL OF THE
ACOUSTICAL SOCIETY OF AMERICA

**Special Issue: Ocean Acoustics
in the Changing Arctic**

The acoustical properties of tetraethyl orthosilicate based granular silica aerogels

H. Begum,^{1,a)} K. V. Horoshenkov,¹ M. Conte,² W. J. Malfait,³ S. Zhao,³ M. M. Koebel,³ P. Bonfiglio,⁴ and R. Venegas⁵

¹Department of Mechanical Engineering, The University of Sheffield, S1 3JD, United Kingdom

²Department of Chemistry, The University of Sheffield, S3 7HF, United Kingdom

³Laboratory for Building Energy Materials and Components, Swiss Federal Laboratories for Materials Science and Technology, Empa, Überlandstrasse 129, 8600, Dübendorf, Switzerland

⁴Materiacustica srl, Via Camilla Ravera 15A, 44122 Ferrara, Italy

⁵University Austral of Chile, Institute of Acoustics, P.O. Box 567, Valdivia, Chile

ABSTRACT:

Available data suggests that granulated aerogels can be of interest in terms of their sound absorption performance in the audio frequency range. However, there is still no thorough understanding of the complex physical phenomena which are responsible for their observed acoustical properties. This work is an attempt to address this gap through advanced material characterization methods and mathematical modelling. Aerogel samples are produced through a two-step, acid-base sol-gel process, with sol silica concentration and density being the main variables. Their pore structure is carefully characterized by nitrogen sorption analysis and scanning electron microscopy. The acoustical properties of hard-backed granular silica aerogels are measured in an impedance tube and the results predicted accurately with the adopted theoretical model. Although silica aerogels have over 90% of open interconnected pores, this was neither reflected in the measured acoustical properties nor the parameter values predicted with the model. Novel results show that only a proportion of the micro and mesopores in the direct vicinity of the grain surface influenced the acoustical properties of aerogels. Further work in the hierarchical pore structure of aerogels is required to better understand the roles of different pore scales on the measured acoustical properties of a granulated aerogel.

© 2021 Author(s). All article content, except where otherwise noted, is licensed under a Creative Commons Attribution (CC BY) license (<http://creativecommons.org/licenses/by/4.0/>). <https://doi.org/10.1121/10.0005200>

(Received 17 February 2021; revised 17 May 2021; accepted 17 May 2021; published online 15 June 2021)

[Editor: Ning Xiang]

Pages: 4149–4158

I. INTRODUCTION

Aerogels have gathered increasing interest from industry in recent years. Their highly porous nature allows sound waves to penetrate far enough into the structure and multiple interactions to take place, making them efficient acoustic absorbers.¹ As a result, they are now used in a broad range of commercial products with potential applications as catalyst supports,² CO₂ adsorbents,³ black material absorbers for solar harvesting,⁴ and drug delivery systems⁵ in the form of bulk materials. These materials behave as membranes⁶ and effective thermal and acoustic insulation materials for industrial installations, pipelines, and buildings.^{2,7} The latter is directly relevant to this work.

Silica aerogels are predominantly mesoporous (2–50 nm pore size) materials in which the liquid part of the gel has been replaced by air, with unique properties such as high porosity (80%–99.8%), low density (0.003–0.5 g cm⁻³), large specific surface area (500–1000 m² g⁻¹)⁸ and outstanding thermal insulation performance.^{2,9} Typical thermal conductivity values are around 0.015 W m⁻¹ K⁻¹, approximately

half of that of standing air (0.026 W m⁻¹ K⁻¹) and much better than that of conventional insulation materials (0.03–0.040 W m⁻¹ K⁻¹).¹⁰ Silica aerogel is available commercially in the form of particles (granulate and powder) and aerogel-fiber blankets. Particulate/granulated aerogels are applied in renders, concrete, cavities, or translucent elements, whereas aerogel blankets can be applied for pipe or building insulation.¹¹ Production methods include supercritical drying (SCD, mostly for blankets) and ambient pressure drying (APD, mostly for granulate and powder).

The thermal insulation properties and the physics of heat transport of aerogels are well studied.¹² However, the acoustical properties are not so well understood. Earlier research on sound propagation in aerogels largely focused on sound velocity as a function of aerogel density^{13,14} which was measured mainly in the ultrasonic frequency range above 20 kHz. Although basic models were proposed to predict the sound speed in aerogel, no attempt was made to account for the frequency-dependent sorption-influenced diffusion in micro- and mesopores. Some later publications in Refs. 15 and 16 extended measurements to the audible frequency range below 20 kHz. For example, the work by Buratti *et al.*¹⁵ used a standard impedance tube setup to

^{a)}Electronic mail: hbegum3@sheffield.ac.uk, ORCID: 0000-0003-2396-8412.

measure the acoustic absorption coefficient and transmission loss of layers of aerogel granules in the frequency range of 100–6400 Hz. However, no theory was proposed to explain the presented data and no attempt was made to relate these data to the physical mechanisms that are responsible for sound attenuation. In fact, a majority of published acoustic studies on aerogels carried out in the audible frequency range were focused on measuring the ability of an aerogel layer to absorb sound or resist sound transmission.^{16–19} Other studies measured the sound speed in and reflection coefficient from a layer of aerogel (e.g., Ref. 20). More recent work by Takeshita *et al.*²¹ estimated the specific pore surface area, peak pore size, and porosity in chitosan aerogels with three different densities. They measured the absorption coefficient of layers of these samples in the frequency range of 500–6500 Hz, illustrating its resonance behavior and some dependence on aerogel microstructure. However, as in the case of the other cited studies, no attempt was made to propose a theory to explain the measured absorption data.^{18,19}

To the best of our knowledge, there is still a lack of understanding of the key relations between the aerogel microstructure and a range of physical mechanisms responsible for the frequency-dependent acoustical properties of aerogel granules. Therefore, the purpose of this work is to attempt to explain the acoustic properties of some specific aerogels, with microstructure parameters measured non-acoustically by using a valid theoretical model that accounts for the complexity of acoustic phenomena in multiscale materials. These and other typical aerogel granule mixes are characterized by a pore size distribution that spans a vast range of scales. We focus on a specific grain size of silica aerogels but introduce some variation in porosity and density that was achieved by changing the sol silica content.

A main novelty of this paper is the use of a well understood model²² that can predict the acoustical properties of rigid frame porous media with a vast range of pore scales (i.e., from macropores to micropores) which are carefully characterised. In this paper, we use the International Union of Pure and Applied Chemistry (IUPAC)²³ recommendation to define pores smaller than 2 nm as *micropores*, pores in the ranges of 2–50 nm as *mesopores*, and pores larger than 50 nm as macropores (inner-particle transport pores). This paper attempts to understand how the presence of these pores contributes to the measured acoustical properties of aerogel in its granular form. Advanced material characterization methods and mathematical modelling are used to explain the measured acoustical properties of aerogels in terms of three characteristic sizes and associated scale porosities. This work paves the way to understanding key physical mechanisms which contribute to the routinely measured acoustical properties of aerogels.

The paper is organized in the following manner. Section II describes the methods to synthesize aerogels and to characterize their microstructure acoustically and non-acoustically. Section III presents the model²² that was used to predict the measured acoustical data. Sections IV and V

TABLE I. Materials and quantities used to prepare PEDS.²⁴

Material	Quantity [g]
TEOS	491.2
Ethanol	88
Water	32
Ethanol	88
Water	32
Sulfuric acid	0.41

present the results and discussion. The conclusions of this work are presented in Sec. VI.

II. MATERIALS AND METHODS

A. Aerogel synthesis

Polyethoxydisiloxane (PEDS)²⁴ a pre-polymerized silica precursor made from tetraethyl orthosilicate (TEOS), water, and sulfuric acid was used for the silica aerogel synthesis. As shown in Table I, TEOS was mixed with half of the final amount of ethanol (95% EtOH, denatured with 5 vol.% isopropyl alcohol) and water, and stirred at 35 °C – 40 °C and 250 rpm for 5 min. In another vessel, the second half of ethanol and water was mixed with 0.41 g of sulfuric acid and this solution was slowly added to the first vessel while stirring over 30 min at room temperature.

Silica aerogels were prepared with variable PEDS content in the sol to produce aerogels with different densities (Table II, i.e., TEOS concentration of 30%, 60%, 90%). These materials were named PEDS E30, PEDS E60, PEDS E90, respectively. We describe the synthesis of the PEDS E30 aerogel as an example. To prepare 30 cm³ of gel, corresponding to a packed volume of 50 cm³ granular aerogel sample, 9 ml PEDS was diluted with 21 ml EtOH and 1 ml distilled water under constant stirring for 5 min at room temperature. Next, 0.36 ml of 5.5 M ammonium hydroxide solution (NH₄OH in water) was then added, and gelation occurred within 3–5 min. The ammonia activated sol was poured into square polystyrene molds with dimensions 5 × 5 × 2 cm³. The gel was covered with an additional 0.4 ml ethanol to prevent solvent evaporation due to exposure to air, which would result in cracking of the gel. All sample boxes were closed with lids and aged for 24 h at 65 °C depending upon the wt.% of SiO₂. The same procedure was carried out for the rest of the samples, adjusting the quantities according to Table II.

TABLE II. The preparation of three standard equivalents at weight percentages of silica (expressed as SiO₂) for samples with TEOS concentration of 30%, 60%, and 90%.²⁵

Sample name	SiO ₂ wt.%	PEDS [mL]	EtOH [mL]	Water [mL]	5.5M NH ₄ OH [mL]
PEDS E30	6	9	21	1	0.36
PEDS E60	12	18	12	1	0.36
PEDS E90	18	27	3	1	0.36

TABLE III. Materials and quantities used to age aerogels.

Material	Quantity [mL]
HMDSO	60
HCl (12 M)	0.34
95% EtOH	2.205

The gels were washed with ethanol twice overnight at 65 °C. To maintain a hydrophobic product and to enable ambient pressure drying, a hydrophobization treatment was carried out to replace the silanol and ethoxy surface groups with hydrophobic trimethylsilyl groups. The aged gels were hydrophobized in a mixture of hexamethyldisiloxane (HMDSO), concentrated hydrochloric acid (12 M), and ethanol at 65 °C for 24 h (Table III).

The hydrophobized gels were dried by APD in a ventilated oven for 3 h at 150 °C. In parallel, monolithic silica aerogel samples were prepared by supercritical CO₂ drying, but the focus of this paper is on the APD granulate. The structure of pure monolithic silica aerogel as a photographic image, drawing, and TEM image to show its pearl-like necklace shape before it shatters into its granular form is shown in Fig. 1.

B. Characterization

The apparent bulk or envelope density was measured from the mass and volume by the powder displacement method (Micrometrics GeoPyc 1360). The specific surface area, S_{BET} was calculated from nitrogen sorption isotherms (Micrometrics 3flex) using Brunauer–Emmet–Teller (BET) analysis.²⁶ The porosity (ϕ) was calculated according to Eq. (1) (e.g., Ref. 27) from the bulk (ρ_b) and skeletal (ρ_s) density, where the skeletal density of 2.0 g cm⁻³ was adopted²⁸ (a typical value for silica aerogel)

$$\phi = 1 - \frac{\rho_b}{\rho_s}. \tag{1}$$

The effective pore size and average pore diameter from adsorption (ads) and desorption (des) data were calculated using the Barrett–Joyner–Halenda (BJH) method.²⁹ The BJH method yields the derivative of pore volume (dV) plotted versus pore width (d_n), i.e., differential distribution plots.³⁰ It is important to note, however, that the BJH

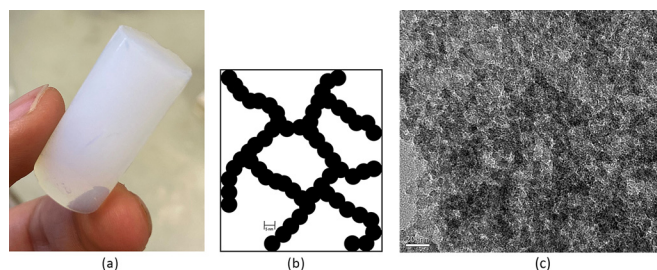


FIG. 1. (Color online) Structure of monolithic silica aerogel as (a) a photographic image, (b) drawing, and (c) TEM image.

method is affected by the mechanical deformation of the aerogel when it undergoes a second drying from purging with liquid nitrogen,³¹ so results should be taken as referential. In addition, nitrogen sorption analysis does not sample pores larger than ~50 nm.

Therefore, the specific pore volume (V_p) and average pore size of the mesopores (D_p) were also evaluated from the density and surface area assuming that the pores are cylindrical,

$$V_p = \frac{1}{\rho_b} - \frac{1}{\rho_s}, \tag{2}$$

$$D_p = \frac{4V_p}{S_{BET}}. \tag{3}$$

Scanning electron microscopy (SEM) images were obtained using a FEI Nova NanoSEM 230 instrument (FEI, Hillsboro, OR) at an accelerating voltage of 10 kV and a minimum working distance of 4.1 mm. Aerogel samples were fixed onto carbon taped stubs and subsequently coated with 15–20 nm platinum for SEM analysis. A Java-based image processing program, ImageJ, was used to manually measure the size of 50 individual pores obtained on a high magnification SEM image. The data were collated to determine their normal approximate of the pore size distribution, see supplementary material at Ref. 32.

The acoustical properties of aerogel samples were measured in a bespoke, 10 mm bore impedance tube³³ to test aerogels made in relatively small batches. This 2-microphone tube setup was developed to test 40 mm³ material specimens in accordance with the standard ISO 10534–2:2001.³⁴ This setup enabled us to measure the surface acoustic impedance, reflection, and absorption coefficient in the frequency range of 300–3000 Hz. The impedance tube was installed in an upright position to allow the acoustic properties of unconsolidated material to be measured accurately. The spacing between the two microphones was 30 mm, which is usual for this frequency range as recommended in the standard.³⁴ A specimen from each granulate sample was deposited through a funnel into a 10 mm diameter, 50 mm deep sample holder (see Fig. 2). The thickness of each specimen in the impedance tube was kept close to 50 mm to ensure reliability. This choice of the sample thickness is typical for commercially available acoustic absorbers such as foams and fiberglass. The choice of the sample thickness is not critical for this work because it is accounted for accurately by the adopted model²² (also see Sec. III). The packed-bed (bulk) density of the material sample was measured and recorded to ensure that the specimen density was controlled within 1%.

This impedance tube setup was calibrated in accordance with the standard method detailed in Ref. 34 and validated against data obtained with larger tube setups for a 50 mm layer of identical glass beads with 1 mm radius. This is a well characterized material³⁵ with solid glass particles whose size is similar to that found in our aerogels so that it was used for a comparison with the results presented in Sec.

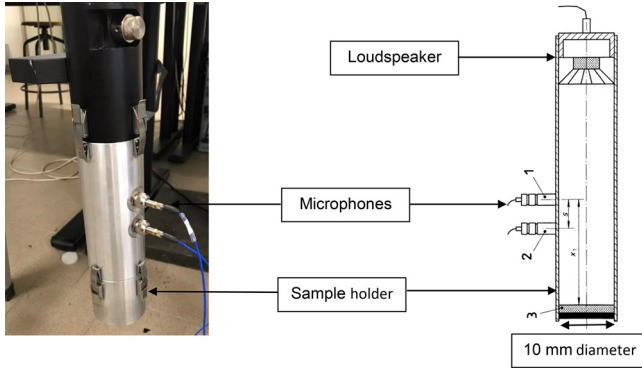


FIG. 2. (Color online) Vertically standing 10 mm impedance tube (adapted from Ref. 34).

IV. Three measurements of each of the three different concentrations of PEDS samples was taken to ensure repeatability which was 1%–2%.

III. MODELLING OF THE ACOUSTICAL PROPERTIES OF AEROGELS

Granular aerogels consist of highly porous particles with a large internal pore surface area. Modelling of their acoustical properties requires accounting for its multiscale nature and physical processes that occur at different scales. In this work, the model proposed by Venegas *et al.*²² is applied. This upscaled analytical model has been developed for an array of spherical porous grains in which two inner-particle scales of porosity are considered. The two different types of inner particle pores are modelled as an array of monodisperse cylindrical inner-particle (transport) pores with size greater or comparable with the mean free path and a network of mesopores modelled as an effective medium where diffusion determines the mass transfer. The model also accounts for the viscosity and heat transfer effects in the voids formed between the particles, rarefied gas flow and heat transfer in the inner-particle transport pores, interscale (voids to/from inner-particle pores) pressure diffusion, interscale (transport- to/from mesopores) mass diffusion, and sorption in the micro- and mesopores. Due to the characteristic sizes of the synthesized granular aerogel samples, it will be shown that the latter has a negligible influence on the acoustic properties of the said samples. The model is based on six parameters which are:²² (i) the effective particle radius (r_p); (ii) the voids porosity (ϕ_p), i.e., porosity related to the proportion of the air space between the aerogel particles; (iii) the inner-particle macropore radius (r_t); (iv) their associated porosity (ϕ_t); (v) the effective diffusion coefficient (D_e) determining the mass transport in the mesopores;³⁵ and (vi) and the effective linearized sorption equilibrium constant (H_e), which can be interpreted as an apparent porosity of the smallest pores (ϕ_n).^{22,36} These, together with other fundamental physical properties of the saturating fluid, are the input parameters to predict the dynamic density (ρ) and the effective compressibility (C) of the effective fluid in the aerogel pores (see Tables I

and II from Ref. 22), which are then used to calculate the complex acoustic characteristic impedance,

$$Z_c = \sqrt{\frac{\rho}{C}}, \quad (4)$$

and wavenumber

$$k_c = \omega \sqrt{\rho C}, \quad (5)$$

which are the function of frequency, ω . Since the effective particle radius is usually millimetric and therefore much larger than the inner-particle submicron pores, the dynamic density, which accounts for viscosity effects in the pores, is well approximated with that of the voids (ρ_p), i.e.,

$$\rho = \frac{\eta}{j\omega k_p} = \rho_p, \quad (6)$$

where k_p is the dynamic viscous permeability of the inter-particle space which is primarily controlled by the particle radius (r_p). Its expression for an array of spherical particles has been introduced in Ref. 37 and can also be found in Table II from Ref. 22.

The effective compressibility of the fluid in the aerogel pores captures a number of effects. These effects include heat transfer in the interparticle voids, rarefied gas flow and heat transfer in the inner-particle transport macropores, interscale pressure, and mass diffusion processes affected by sorption. Following the original definitions,²² the effective compressibility is

$$C = C_p + (1 - \phi_p)C_{mn}F_{pmn}, \quad (7)$$

where C_p is the effective compressibility of the fluid that saturates the interparticle voids. The other terms in Eq. (7) are

$$C_{mn} = C_m + (1 - \phi_m)C_nF_{mn}, \quad (8)$$

which is the compressibility of the effective fluid in the macro- and mesopores in the aerogel particles, C_m is the effective compressibility of the fluid that saturates the macropores, and C_n is the compressibility of the fluid that saturates the mesopores. The function F_{pmn} and F_{mn} describe the pressure and mass diffusion processes, respectively. These quantities are complex, frequency-dependent, and controlled by the fundamental properties of the saturating fluid and parameters r_p , ϕ_p , r_t , ϕ_t , D_e , and H_e . Their analytical expressions can be found in Table I from Ref. 22. We do not present the full 6-parameter model here for brevity.

Equations (4) and (5) can be used to predict the surface impedance of a hard-backed layer of aerogel, which is typically measured using the standard impedance tube method as described in Sec. II. The surface impedance of a hard-backed layer of aerogel of thickness d is

$$Z_s = -jZ_c \cot(k_c d), \quad (9)$$

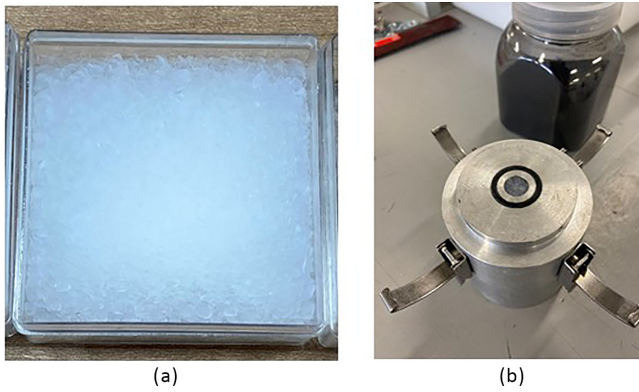


FIG. 3. (Color online) Photographs of the 50 mm × 50 mm container with granular silica aerogel 2–3 mm sieved mix (left) and 40 mm³ of it in the 10 mm diameter, 50 mm deep impedance tube sample holder (right).

where $j = \sqrt{-1}$. The normalized surface impedance,

$$z = \frac{Z_s}{\rho_0 c_0}, \tag{10}$$

can then be used to predict the frequency-dependent, normal incidence pressure reflection coefficient,

$$R = \frac{z - 1}{z + 1}, \tag{11}$$

where ρ_0 and c_0 are the ambient density of air and sound speed in air, respectively. The acoustic absorption coefficient of this layer is

$$\alpha = 1 - |R|^2. \tag{12}$$

The quantities predicted with Eqs. (9)–(11) are complex and frequency-dependent quantities, and their behavior is rarely explained theoretically in the published literature of aerogels. The absorption coefficient predicted with Eq. (12) is a real, frequency-dependent quantity that is often quoted in research on acoustical properties of aerogels (e.g., Refs. 15 and 16), but rarely predicted.

IV. RESULTS AND DISCUSSION

A. Density, nitrogen sorption analysis, and microstructure

TEM analysis confirms the pearl-like necklace type structure typical for silica aerogels (Fig. 1). During APD, the gel bodies fractured into mm-sized granules, which were sieved to select particle sizes between 2 and 3 mm for further analysis (Fig. 3). Figure 4 shows that these particles are not spherical as assumed in the model presented in Sec. III, but angular, with sharp edges and some resembling platelets. Much smaller fractions are also present in these images suggesting that this material is fragile and can crumble. The presence of smaller particle fractions is likely to affect the measured acoustical properties as it will be illustrated in part B. The analysis of these images suggests that the size of the particles in the mix PEDS E90 is relatively smaller than that in the other two mixes.

The pore size and microstructure were analyzed for three different aerogels prepared with three different PEDS concentrations of TEOS vol.% 30%, 60%, and 90%. Note that the accurate determination of aerogel pore size distributions is not a trivial task. SEM image analysis is particularly sensitive to meso- and macropores, but not to micropores. In addition, manual peak-picking is subject to sampling bias, the imaged fracture surfaces may not be representative of the bulk, and the coating and contrast/brightness settings may affect the results. In contrast, nitrogen sorption analysis does probe the bulk of the material but is not sensitive to macroporosity (> 50 nm). In addition, sample deformation during nitrogen sorption can affect the pore size. Finally, simple approximations of average pore size rely on simplistic approximations of meso- and micropore pore geometry, e.g., cylindrical [see Eq. (3)], and it does not fully capture the complexity of the real aerogel pore structure.

Using SEM images and ImageJ software the average pore size of the normal distributions derived by manually estimating pore diameters of PEDS E30 is 45 nm, PEDS E60 is 33 nm and PEDS E90 is 27 nm (Fig. 5). Pore size distribution data calculated by individually measuring the diameter of the pore from SEM using ImageJ are provided as supplementary data.³²

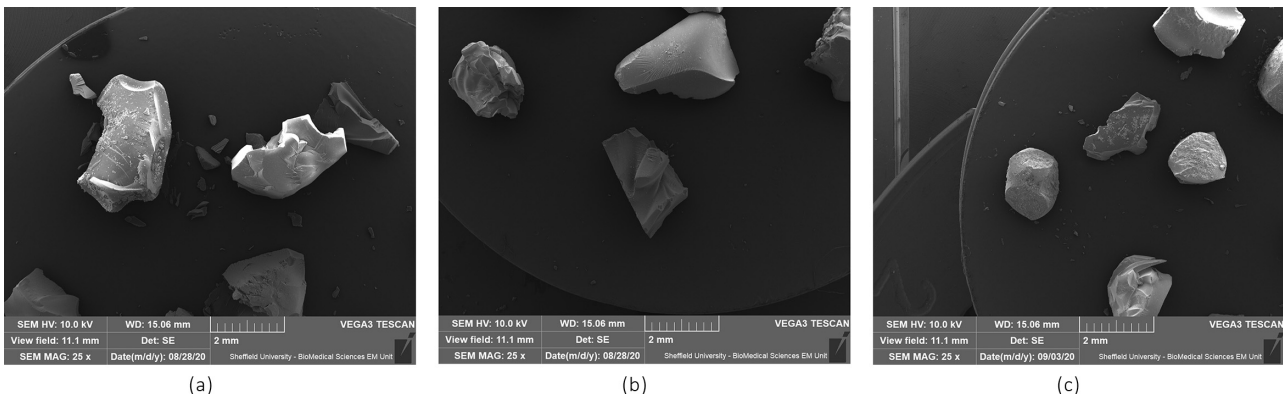


FIG. 4. SEM images of micrometric grains of the 2–3 mm fraction of (a) PEDS E30, (b) PEDS E60, (c) PEDS E90.

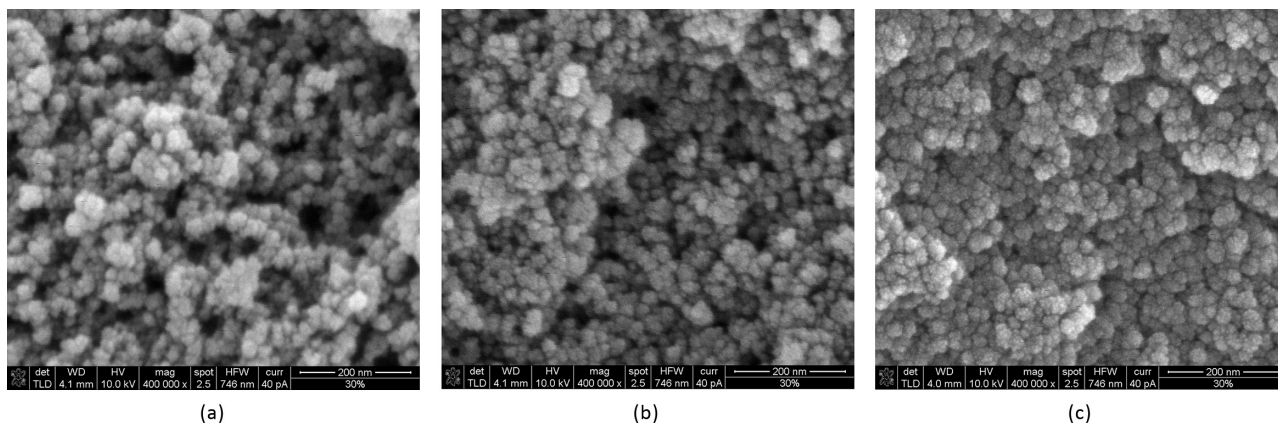


FIG. 5. Analysis of the size of 50 individual pores using ImageJ software applied to SEM images of (a) PEDS E30, (b) PEDS E60, (c) PEDS E90.

All aerogels, prepared with variable PEDS concentration and hence variable final bulk densities, display type IV nitrogen isotherms²⁹ typically observed for silica aerogel (Fig. 6). The distributions of pore widths obtained from these histograms obtained with the BJH method can be found in the supplementary data.³² The smallest maximum frequency counts obtained for the BJH pore width (desorption) for PEDS E30, PEDS E60, and PEDS E90 specimens were 3.67, 6.94, and 5.78 nm, respectively. These were estimated from the desorption data.³² The largest maximum frequency counts obtained for the BJH pore width (adsorption) for PEDS E30, PEDS E60, and PEDS E90 specimens' aerogels was 11.27, 28.87, and 15.34 nm, respectively. These were estimated from the adsorption isotherms.³² It is seen that during desorption there is a smaller distribution of pore sizes than during adsorption. This may be due to ink-bottle pores (see Fig. 7 from Ref. 38), or interconnected pores of complex geometry, where the condensation pressure within the cavity is smaller than the evaporation pressure as the presence of condensed liquid in the constriction helps to nucleate the liquid phase.³⁹ As consistent with the hysteresis loop observed in Figs. 6(a)–6(c). In this case, when the pressure of capillary evaporation is reached in the small pore opening, the whole pore is emptied through a desorption percolation⁴⁰ process leading to an artificially narrow pore size distribution.

Table IV lists key parameters for these three aerogels. Both the SEM data and the calculated pore sizes [Eq. (3)]

display the expected monotonic decrease in average pore width with increasing PEDS concentration and density. In contrast, the BJH average pore widths are highest at intermediate densities, presumably because of the limitations with sample deformation and macroporosity during nitrogen sorption analysis (see Sec. II B).

B. Acoustical properties

Figure 8 illustrates the absorption coefficient spectra for the 50 mm layer of glass beads and three layers of granular aerogels developed in this work. This example illustrates well the effect of micropores, which is a clear shift in the frequency of the first destructive interference maximum in the material layer towards the lower frequency range. This shift is associated with a relative decrease in the sound speed in aerogel which is caused by an increase in dynamic compressibility (or reduced dynamic bulk modulus) of the air in the material pores. This is mainly a result of the pressure diffusion effect in the inner-particle pores. This effect is more pronounced for aerogel PEDS E90 with a smaller pore width (see Table IV). Above the interference maximum, the absorption coefficient depends less on the compressibility and more on the viscous permeability of aerogel. In this frequency range, the higher absorption coefficient is for the mix PEDS E90 because it is composed of slightly

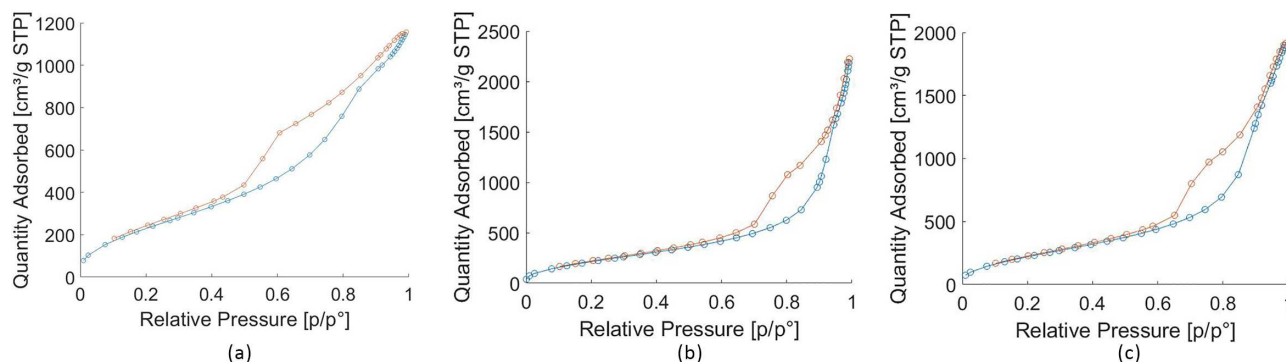


FIG. 6. (Color online) BET isotherm linear plots of (a) PEDS E30, (b) PEDS E60, (c) PEDS E90.

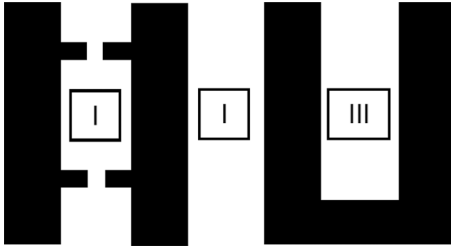


FIG. 7. Schematic for three generic types of pores, (i) ink bottle, (ii) straight with both ends open, and (iii) straight with only one end open.

smaller particles (see Fig. 4), so that its permeability is smaller than that of the other two aerogel mixes.

In order to explain the acoustical absorption behavior shown in Fig. 8, the complex reflection coefficient data for the three aerogels and theoretical model described in Sec. III were used to invert the parameters of the model: r_p , ϕ_p , r_t , ϕ_t , D_e , and H_e . The differential evolution algorithm⁴¹ was used in the fitting process. It enabled us to determine the best set of the non-acoustical parameters to find the minimum of the following objective function:

$$G(x) = \sum_{m=1}^M \left| R^{(t)}(x, \omega_m) - R^{(e)}(\omega_m) \right|^2, \quad (13)$$

where M is the number of frequency points (ω_m) in the measured reflection coefficient spectrum $R^{(e)}(\omega_m)$ and $x = [r_p, \phi_p, r_t, \phi_t, D_e, H_e]$ is the design variable vector. In Eq. (13), $R^{(t)}(x, \omega_m)$ is the reflection coefficient predicted with Eq. (11) for the given values of frequency and non-acoustical parameters in the design vector. This minimization procedure was carried out in the frequency range of 300–3000 Hz for $M = 448$ frequency points. The fundamental properties of air were taken as their ambient values at 20 °C.

The inversion algorithm was initially tested on a layer of loosely packed non-porous glass beads with nominal

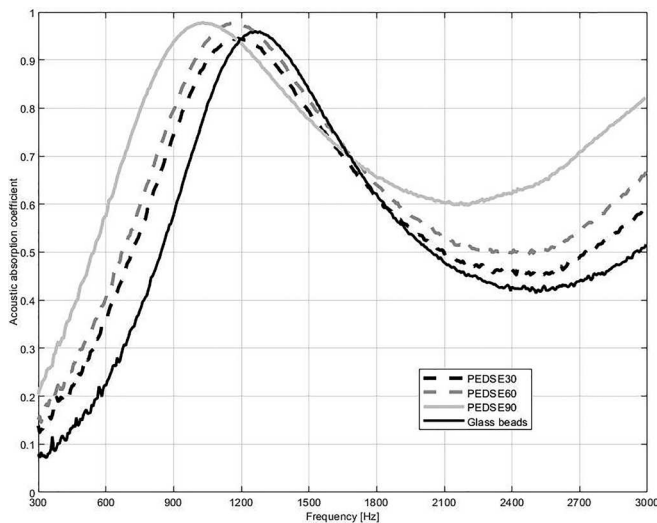


FIG. 8. The measured absorption coefficient spectra for a nominal 50 mm hard-backed layer of the four materials studied in this work.

TABLE IV. Properties of density, pore structures, surface area, adsorption (ads), and desorption (des) coefficients of silica aerogels for PEDS E30, PEDS E60, and PEDS E90.

Properties	PEDS E30	PEDS E60	PEDS E90
ρ_b [g cm ⁻³]	0.130	0.163	0.227
ρ_s [g cm ⁻³]	2	2	2
ϕ , porosity %	93.5	91.9	88.7
S_{BET} [m ² g ⁻¹]	946	885	917
d_n , nm			
BJH ads	3.67	6.94	5.78
BJH des	11.27	28.87	15.34
SEM	45.3	33.1	27.4
$4V_{pore}/S_{BET}$	30.5	25.6	17.1

particle diameter of 2 mm and a thickness of 50 mm, respectively. This is a well characterized material (e.g., Ref. 35). Note that since the beads are non-porous, the model used corresponds to that of a packing of solid particles,^{37,42} i.e., $\rho = \rho_p$ and $C = C_p$. Figure 9 presents the measured and predicted spectra of the complex reflection coefficient for a 50 mm layer of glass beads. The mean error between the model and data is less than 5.5%, which suggests a close fit. This fit was achieved with the following values of the non-acoustical parameters: $r_p = 0.95$ mm, $\phi_p = 0.4$, and $d = 53.4$ mm. Using the measured acoustical data, the value of the inverted void porosity is close to that expected^{42–44} from a loose packing of identical beads ($0.32 \leq \phi_p \leq 0.45$). The particle radius is also on the order of its nominal value provided by the glass bead manufacturer. The value of the layer thickness d used in this model was slightly larger than the nominal value and corresponds to approximately a single extra layer of particles. This trend was also observed in Ref. 42 for a packing of non-porous lead shots. The slight disagreement between the data and the predictions could be due to the fact that the used model does not account for the exact particle arrangement but models the dynamic density and effective compressibility by making use of a self-consistent approach in which the packing condition is accounted for in a generic way as discussed in detail in Refs. 37 and 42. It is clear, however, that the physics is well captured by the model.

With the model validated against the glass beads data, the parameter inversion algorithm was applied to the reflection coefficient data measured with the impedance tube to determine the non-acoustical parameters characteristic to the aerogel’s granular mixes produced in this work. The results of this inversion are summarized in Table V.

Figure 10 show examples of the agreement between the measured and predicted acoustical surface impedance spectra. The relative mean error between these data and predictions was generally less than 3.1%, suggesting that the model captures the acoustical behavior of aerogels accurately. Here, the error is lower compared to that found for glass beads due to the higher number of fit parameters used to predict the acoustical properties of the aerogel mixes.

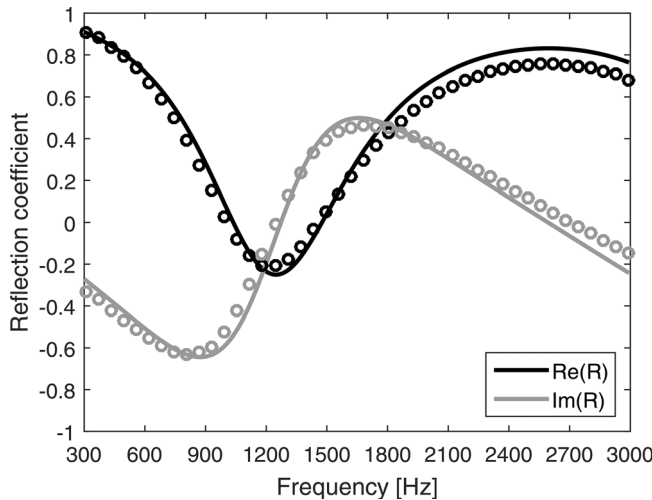


FIG. 9. Model validation. The measured (circles) and predicted (lines) reflection coefficient for a hard-backed layer of loosely packed glass beads.

V. DISCUSSION

The values of the inverted parameters for aerogel pore microstructure (Tables IV and V) make physical sense. For example, the particle radius (r_p) is smaller than the nominal value, which can be explained by the non-spherical shape of the particles and the expected presence of small particles, such as those shown in Fig. 4, that may sit in between the larger particles. The values of the void porosity (ϕ_p) are in the range 0.35–0.45, which are expected values for packings of non-spherical grains (see Refs. 43 and 44). The radius of the macropores is on the order of $1\ \mu\text{m}$, which is a typical value for this type of transport pores (see Refs. 42, 45, and 46) for the case of activated carbons). The existence of the small but non-negligible transport porosity (ϕ_t) ensures that the fluid saturating molecules are transported to the smaller inner-grain pores and influences the effects of pressure and mass diffusion in the material.^{22,36,42} The acoustic measurements also show that the overall porosity of aerogels is not as high as the one measured non-acoustically. This can be seen by looking at the low-frequency limit of the imaginary part of the surface impedance. Figure 11 shows that the porosity inverted from acoustical data is around 0.60–0.65 for the three aerogel samples.

The mesopore radius, measured from the SEM images, for the samples PEDS E30, PEDS E60, and PEDS E90 are 22.7, 16.8, and 13.7 nm, respectively. For mesopores of this size, the theory developed in Refs. 22 and 36 predicts that the effects of sorption on the acoustical properties of the material

TABLE V. The results of the inversion of the three materials studied in this work.

Material	r_p [mm]	ϕ_p	r_t [μm]	ϕ_t	D_e [$\mu\text{m}^2\ \text{s}^{-1}$]	H_e	d [mm]
PEDS E30	0.85	0.45	1.50	0.059	0.99	0.18	52.9
PEDS E60	0.80	0.45	1.19	0.074	0.80	0.17	52.4
PEDS E90	0.70	0.36	1.50	0.079	0.60	0.16	52.9

are negligible and that the effective linearized sorption equilibrium constant reduces to the apparent porosity of the smallest pores in the grains, i.e., $H_e = \phi_n$. Moreover, at normal conditions, the transport mechanism that dominates the behavior in the nanopores is Knudsen diffusion.⁴⁶ Therefore, the effective diffusion coefficient is determined by the Knudsen diffusion coefficient, i.e., $D_e = D_k$, which for an array of cylindrical nanopores can be assessed as Ref. 45,

$$D_e = \frac{2\phi_n r_n v}{3}, \quad (14)$$

where v is the thermal velocity. Making use of the D_e data in Table V and Eq. (14) yields the nanopore radius of 17.7, 15.4, and 12.3 nm for the samples PEDS E30, PEDS E60, and PEDS E90, respectively. These nanopore radius values are close to those measured from the SEM images (see Table IV). The overall porosity estimated from

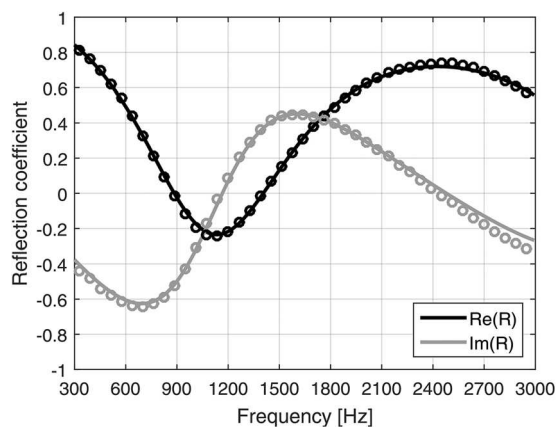
$$\phi = \phi_p + (1 - \phi_p)(\phi_t + (1 - \phi_t)\phi_n), \quad (15)$$

and porosity data given in Table V is 0.577, 0.576, and 0.503 for the samples PEDS E30, PEDS E60, and PEDS E90, respectively. These are 30%–40% lower than those measured directly (see Table IV). Silica aerogels usually have close to 100% open porosity measured with He pycnometry so that the inner-particle pores should remain open for the incident sound wave. However, this is not reflected in the porosity values inverted using the measured acoustical data and proposed sound propagation model. One can argue that only a proportion of the micro- and mesopore pore length, which is in the direct vicinity of the transport pores or grain surface, may influence the acoustical properties of the produced aerogels. This remains an open question.

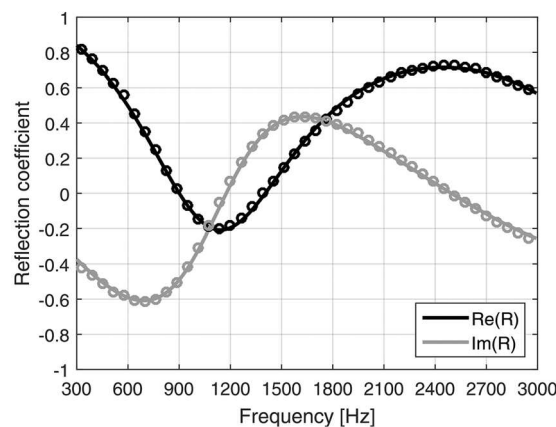
In summary, the produced aerogels can be considered as triple porosity nonsorptive materials in which the sound dissipation is determined by viscosity and heat transfer effects in the voids formed between the particles, rarefied gas flow and heat transfer in the inner-particle transport pores, inter-scale (voids to/from inner-particle pores) pressure diffusion and inter-scale (transport- to/from mesopores) mass diffusion.

VI. CONCLUSIONS

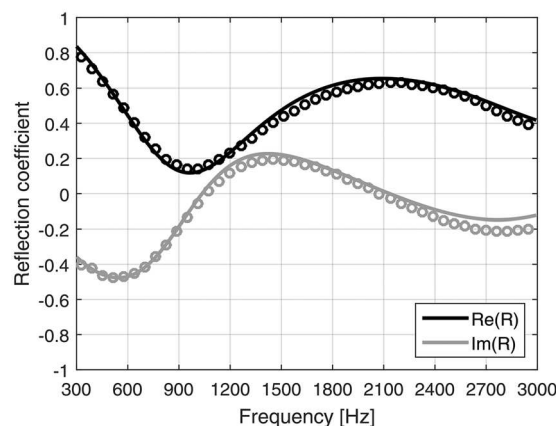
In this work, three granular aerogel formulations were produced, and their microstructural and acoustical properties were measured using a range of characterization methods. The acoustical properties were predicted using the model by Venegas *et al.*,^{22,36} an inversion method based on experimental data and function minimization [Eq. (13)]. It is a main novelty of this work because there is a general lack of understanding of how to predict and interpret the measured acoustical behavior of granular aerogels. The theoretical model adopted in this work considers three scales of heterogeneities where different physical phenomena affect sound propagation. Such a model explains that the dissipation of sound in the studied granular aerogels is due to viscous and



(a)



(b)



(c)

FIG. 10. Examples of the measured and predicted reflection coefficient for hard-backed layers of aerogel granulate. (a) PEDS E30, (b) PEDS E60, (c) PEDS E90.

thermal effects in the voids, rarefied gas flow and heat transfer in the inner-particle transport macropores, inter-scale (voids to/from inner-grain pores) pressure diffusion, and inter-scale (transport- to/from meso pores) mass diffusion, with the latter two largely influencing the acoustic absorption behavior at the lower frequencies of sound. These are controlled by the presence of transport and mesopores in the material grains. It is shown that the absorption coefficient of

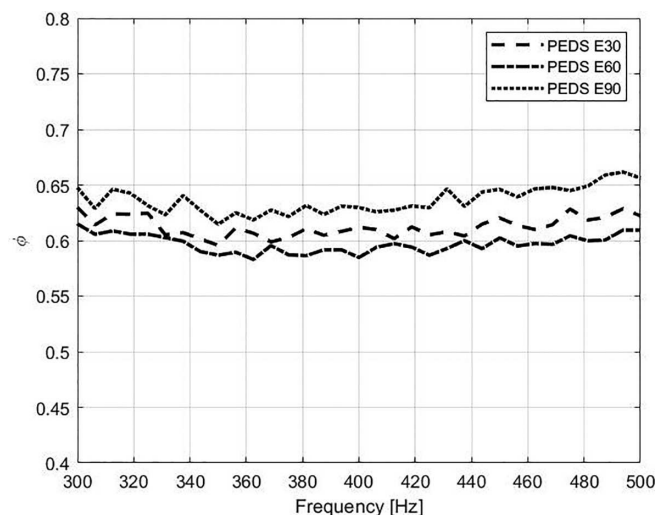


FIG. 11. Acoustically determined porosity for PEDS E30, PEDS E60, and PEDS E90.

these materials increases significantly due to the presence of pores whose scale is comparable with the mean free path. This is explained by an increase in the complex compressibility (reduced bulk modulus) of air in the inner-particle pores due to the said diffusion effects.

Chemical modification allowed us to produce aerogels with inner-particle microstructure that was well characterized using SEM and BJH methods. This work showed that the wt.% of silica has an effect on the pore structure. There was some decrease in the width of mesopores and increase in the proportion of the so-called transport pores on the particle surface leading to the mesopores in PEDS E90 aerogel. The overall porosity inverted from the experimental acoustical data was found to be 30%–40% lower than the values measured directly *via* the material density estimate. The fact the aerogels usually consist of fully interconnected pores is not reflected in the pore parameter values inverted using the experimental acoustical data and adopted sound propagation model. It is likely that only a proportion of the mesopore length in the direct vicinity of the transport pores or grain surface may influence the acoustical properties of the produced aerogels. This remains an open question and naturally suggests that more research is needed to understand better the relative roles of macro-, meso-, and micropores on the acoustical properties of aerogels. In particular, it is of research interest to understand the effective path length along the meso- and macropores that contributes to the measured acoustical properties of aerogels.

ACKNOWLEDGMENTS

The authors would like to thank the EPSRC-sponsored Centre for Doctoral Training in Polymers, Soft Matter and Colloids (EP/L016281/1) at The University of Sheffield for their financial support of this work. We would also like to acknowledge our industry partner Armacell and Dr. Mark Swift and Mr. Pavel Holub for their continued support throughout this research study. R.V. acknowledges partial

support from Corporación de Fomento de la Producción CORFO Chile (Production Development Corporation) through Grant No. 16ENI2-66903 Innoving2030.

- ¹M. A. Kuczmariski, J. C. Johnston, “Acoustic absorption in porous materials,” NASA/TM—2011-216995, www.sti.nasa.gov (Last viewed April 27, 2021).
- ²G. Reichenauer, A. M. Aegerter, N. Leventis, and M. M. Koebel, “History of aerogels,” *Aerogels Handbook* (Springer, New York, 2011), Chap. 1.
- ³S. Cui, W. Cheng, X. Shen, M. Fan, A. Russell, Z. Wu, and X. Yi, “Mesoporous amine-modified SiO₂ aerogel: A potential CO₂ sorbent,” *Energy Environ. Sci.* **4**, 2070–2074 (2011).
- ⁴W. Sun, A. Du, Y. Feng, J. Shen, S. Huang, J. Tang, and B. Zhou, “Super black material from low-density carbon aerogels with subwavelength structures,” *ACS Nano*, **10**, 9123–9128 (2016).
- ⁵Z. Ulker and C. Erkey, “An emerging platform for drug delivery: Aerogel based systems,” *J. Controlled Rel.* **177**, 51–63 (2014).
- ⁶A. A. Fernández-Marin, N. Jiménez, J.-P. Groby, J. Sánchez-Dehesa, and V. Romero-García, “Aerogel-based metasurfaces for perfect acoustic energy absorption,” *Appl. Phys. Lett.* **115**, 061901 (2019).
- ⁷R. G. Martínez, E. Goiti, G. Reichenauer, S. Zhao, M. M. Koebel, and A. Barrio, “Thermal assessment of ambient pressure dried silica aerogel composite boards at laboratory and field scale,” *Energy Build.* **128**, 111–118 (2016).
- ⁸N. Hüsing and U. Schubert, “Aerogels—Airy materials: Chemistry, structure and properties,” *Angew Chem. Int. Ed.* **37**, 22–45 (1998).
- ⁹C. Li, X. Cheng, Z. Li, Y. Pan, Y. Huang, and L. Gong, “Mechanical, thermal and flammability properties of glass fiber film/silica aerogel composites,” *J. Non-Cryst. Sol.* **457**, 52–59 (2017).
- ¹⁰M. M. Koebel, A. Rigacci, and P. Achard, “Aerogel-based thermal super-insulation: An overview,” *J. Sol-Gel Sci. Technol.* **63**, 315–339 (2012).
- ¹¹M. Ganobjak, S. Brunner, and J. Wernery, “Aerogel materials for heritage buildings: Materials, properties and case studies,” *J. Cult. Herit.* **42**, 81–98 (2020).
- ¹²Y. L. He and T. Xie, “Advances of thermal conductivity models of nanoscale silica aerogel insulation material,” *Appl. Therm. Eng.* **81**, 28–50 (2015).
- ¹³J. Gross, J. Fricke, and L. Hrubesh, “Sound propagation in SiO₂ aerogels,” *J. Acoust. Soc. Am.* **91**(4), 2004–2006 (1992).
- ¹⁴L. Forest, V. Gibiat, and T. Woignier, “Biot’s theory of acoustic propagation in porous media applied to aerogels and alcogels,” *J. Non-Cryst. Sol.* **225**, 287–292 (1998).
- ¹⁵V. Gibiat, O. Lefeuvre, T. Woignier, J. Pelous, and J. Phalippou, “Acoustic properties and potential applications of silica aerogels,” *J. Non-Cryst. Sol.* **186**, 244–255 (1995).
- ¹⁶C. Buratti, F. Merli, and E. Moretti, “Aerogel-based materials for building applications: Influence of granule size on thermal and acoustic performance,” *Energy Build.* **152**, 472–482 (2017).
- ¹⁷F. Merli, A. M. Anderson, M. K. Carroll, and C. Buratti, “Acoustic measurements on monolithic aerogel samples and application of the selected solutions to standard window systems,” *Appl. Acoust.* **142**, 123–131 (2018).
- ¹⁸S. Malakooti, H. G. Churu, A. Lee, T. Xu, H. Luo, N. Xiang, C. Sotiriou-Leventis, N. Leventis, and H. Lu, “Sound insulation properties in low-density, mechanically strong and ductile nanoporous polyurea aerogels,” *J. Non-Cryst. Sol.* **476**, 36–45 (2017).
- ¹⁹S. Malakooti, H. G. Churu, A. Lee, S. Rostami, S. J. May, S. Ghidei, F. Wang, Q. Lu, H. Luo, N. Xiang, C. Sotiriou-Leventis, N. Leventis, and H. Lu, “Sound transmission loss enhancement in an inorganic-organic laminated wall panel using multifunctional low-density nanoporous polyurea aerogels: Experiment and modeling,” *Adv. Eng. Mater.* **20**(6), 1700937 (2018).
- ²⁰L. Forest, V. Gibiat, and A. Hooley, “Impedance matching and acoustic absorption in granular layers of silica aerogels,” *J. Non-Cryst. Sol.* **285**, 230–235 (2001).
- ²¹S. Takeshita, S. Akasaka, and S. Yoda, “Structural and acoustic properties of transparent chitosan aerogel,” *Mater. Lett.* **254**, 258–261 (2019).
- ²²R. Venegas, C. Boutin, and O. Umnova, “Acoustics of multiscale sorptive porous materials,” *Phys. Fluids* **29**(8), 082006 (2017).
- ²³K. S. W. Sing, D. H. Everett, R. A. W. Haul, L. Moscou, R. A. Pierotti, J. Rouguérol, and T. Siemieniewska, “Reporting physisorption data for gas/solid systems with special reference to the determination of surface area and porosity,” *Pure Appl. Chem.* **57**(4), 603–619 (1985).
- ²⁴G. M. Pajonk, E. Elaloui, P. Achard, B. Chevalier, J.-C. Chevalier, and M. Durant, “Physical properties of silica gels and aerogels prepared with new polymeric precursors,” *J. Non-Cryst. Sol.* **186**, 1–8 (1995).
- ²⁵S. Iswar, W. J. Malfait, S. Balog, F. Winnefeld, M. Lattuada, and M. M. Koebel, “Effect of aging on silica aerogel properties,” *Micropor. Mesopor. Mater.* **241**, 293–302 (2017).
- ²⁶S. Brunauer, P. H. Emmett, and E. Teller, “Adsorption of gases in multimolecular layers,” *J. Am. Chem. Soc.* **60**, 309–319 (1938).
- ²⁷H.-Y. Nah, V. G. Parale, K.-Y. Lee, H. Choi, T. Kim, C.-H. Lim, J.-Y. Seo, Y. S. Ku, J.-W. Park, and H.-H. Park, “Silylation of sodium silicate-based silica aerogel using trimethylethoxysilane as alternative surface modification agent,” *J. Sol-Gel Sci. Technol.* **87**, 319–330 (2018).
- ²⁸A. Ayrál, J. Phalippou, and T. Woignier, “Skeletal density of silica aerogels determined by helium pycnometry,” *J. Mater. Sci.* **27**, 1166–1170 (1992).
- ²⁹E. P. Barrett, L. G. Joyner, and P. P. Halenda, “The determination of pore volume and area distributions in porous substances. I. Computations from nitrogen isotherms,” *J. Am. Chem. Soc.* **73**, 373–380 (1951).
- ³⁰H. Tian, L. Pan, X. Xiao, R. W. T. Wilkins, Z. Meng, and B. Huang, “A preliminary study on the pore characterization of Lower Silurian black shales in the Chuandong Thrust Fold Belt, southwestern China using low pressure N₂ adsorption and FE-SEM methods,” *Mar. Petrol. Geol.* **48**, 8–19 (2013).
- ³¹G. Reichenauer, M. A. Aegerter, N. Leventis, and M. M. Koebel, “Structural characterization of aerogels,” in *Aerogels Handbook* (Springer, New York, 2011), Chap. 21, 480–482.
- ³²Available online at <https://www.scitation.org/doi/suppl/10.1121/10.0005200> (Last accessed on November 5, 2021).
- ³³MATERIACUSTICA SRL, “Measurement kit for acoustical complex properties testing,” http://www.materiacustica.it/mat_UKProdotti_MAA.html (Last viewed January 27, 2021).
- ³⁴ISO10534-2, 1998: *Acoustics—Determination of Sound Absorption Coefficient and Impedance in Impedance Tubes—Part 2: Transfer-Function Method* (International Organisation for Standardization, Geneva, Switzerland, 1998).
- ³⁵K. V. Horoshenkov, A. Hurrell, and J.-P. Groby, “A three-parameter analytical model for the acoustical properties of porous media,” *J. Acoust. Soc. Am.* **145**(4), 2512–2517 (2019).
- ³⁶R. Venegas and C. Boutin, “Acoustic of sorptive porous materials,” *Wave Motion* **68**, 162–181 (2017).
- ³⁷C. Boutin and C. Geindreau, “Estimates and bounds of dynamic permeability of granular media,” *J. Acoust. Soc. Am.* **124**, 3576–3593 (2008).
- ³⁸A. P. Malanoski and F. van Swol, “Lattice density functional theory investigation of pore shape effects. II. Adsorption in collections of non-interconnected pores,” *Phys. Rev. E* **66**, 041603 (2002).
- ³⁹B. Coasne, A. Galarneau, R. J. M. Pellenq, and F. D. Renzo, “Adsorption, intrusion and freezing in porous silica: The view from the nanoscale,” *Chem. Soc. Rev.* **42**, 4141–4171 (2013).
- ⁴⁰N. A. Seaton, “Determination of the connectivity of porous solids from nitrogen sorption measurements,” *Chem. Eng. Sci.* **46**, 1895–1909 (1991).
- ⁴¹K. Price, R. Storn, and J. Lampinen, *Differential Evolution: A Practical Approach to Global Optimization* (Springer-Verlag, Berlin, 2005).
- ⁴²R. Venegas and O. Umnova, “Acoustical properties of double porosity granular materials,” *J. Acoust. Soc. Am.* **130**(5), 2765–2776 (2011).
- ⁴³W. Man, A. Donev, F. Stillinger, M. T. Sullivan, W. B. Russel, D. Heeger, S. Inati, S. Torquato, and P. M. Chaikin, “Experiments on random packings of ellipsoids,” *Phys. Rev. Lett.* **94**, 198001 (2005).
- ⁴⁴A. Wouterse, S. R. Williams, and A. P. Philipse, “Effect of particle shape on the density and microstructure of random packings,” *J. Phys. Condens. Matter.* **19**, 406215 (2007).
- ⁴⁵D. D. Do, *Adsorption Analysis: Equilibria and Kinetics* (Imperial College Press, London, 1998), p. 892.
- ⁴⁶R. Venegas and O. Umnova, “Influence of sorption on sound propagation in granular activated carbon,” *J. Acoust. Soc. Am.* **140**(2), 755–766 (2016).